

**NANO EXPRESS**

**Open Access**



# Hydrothermal Synthesis and Photocatalytic Property of $\beta$ -Ga<sub>2</sub>O<sub>3</sub> Nanorods

L. Sivananda Reddy, Yeong Hwan Ko and Jae Su Yu\*

## Abstract

Gallium oxide (Ga<sub>2</sub>O<sub>3</sub>) nanorods were facilely prepared by a simple hydrothermal synthesis, and their morphology and photocatalytic property were studied. The gallium oxide hydroxide (GaOOH) nanorods were formed in aqueous growth solution containing gallium nitrate and ammonium hydroxide at 95 °C of growth temperature. Through the calcination treatment at 500 and 1000 °C for 3 h, the GaOOH nanorods were converted into single crystalline  $\alpha$ -Ga<sub>2</sub>O<sub>3</sub> and  $\beta$ -Ga<sub>2</sub>O<sub>3</sub> phases. From X-ray diffraction analysis, it could be confirmed that a high crystalline quality of  $\beta$ -Ga<sub>2</sub>O<sub>3</sub> nanorods was achieved by calcinating at 1000 °C. The thermal behavior of the Ga<sub>2</sub>O<sub>3</sub> nanorods was also investigated by differential thermal analysis, and their vibrational bands were identified by Fourier transform infrared spectroscopy. In order to examine the photocatalytic activity of samples, the photodegradation of Rhodamine B solution was observed under UV light irradiation. As a result, the  $\alpha$ -Ga<sub>2</sub>O<sub>3</sub> and  $\beta$ -Ga<sub>2</sub>O<sub>3</sub> nanorods exhibited high photodegeneration efficiencies of 62 and 79 %, respectively, for 180 min of UV irradiation time.

**Keywords:** Gallium oxides; Nanostructures; Chemical synthesis; Photocatalytic properties

## Background

In recent years, various fabrication methods of photocatalytic products have been developed for the photodegradation of organic and inorganic pollutants in the environment [1, 2]. Particularly, inorganic semiconductor nanomaterials have been considered to be promising for photocatalyst applications because they provide good physical and chemical properties with large surface area, and a variety of morphologies, such as nanorods, cubes, spheres, and flowers, could be achieved by the chemical synthesis [3–8]. In addition to the morphology and surface area of particles, the other factors which can influence the catalytic activity are pore volume, pore size, crystallinity, defect sites, exposed facets, etc. The electron transport mechanism and the exposed facets are related to the morphology of particles. In the one-dimensional (1D) morphology, the generation of electron charge carriers is higher along the elongated nanostructures and gives rise to fast transport of charge carriers, due to the hampering of recombination of charge carriers. Hence, 1D nanostructures are gaining

more importance for their use in different applications as seen by latest reports [9, 10]. For example, Liu et al. studied the morphology-dependent photocatalytic properties of bare zinc oxide nanocrystals [11], which indicated that the rod-shaped ZnO nanostructures have higher photocatalytic activity than the multi-layer disks or truncated hexagonal cones. Similarly, Han et al. also studied the morphology-related properties of nano/microstructured ZnO crystallites [12]. Gallium oxide (Ga<sub>2</sub>O<sub>3</sub>) nanostructures have been recognized as an important material for several applications including catalysts, gas sensors, solar cells, and photodetectors due to their wide bandgap energy ( $E_g = 4.2$  to 4.7 eV) and good luminescence properties [13–16]. Typically, the Ga<sub>2</sub>O<sub>3</sub> nanostructures could be obtained by calcination of gallium oxide hydroxide (GaOOH) which has been synthesized via various fabrication routes including thermal evaporation, hydrothermal, sol-gel, and microwave-assisted methods [17–19].

In order to obtain such GaOOH nanostructures by using a facile hydrothermal method, gallium nitrate was chemically reacted with various alkalis such as NaOH, NH<sub>4</sub>OH, KOH, and Na<sub>2</sub>CO<sub>3</sub> [20, 21]. Then, the phase of the GaOOH nanostructures was changed into the rhombohedral crystal structure ( $\alpha$ -Ga<sub>2</sub>O<sub>3</sub>) and monoclinic

\* Correspondence: jsyu@khu.ac.kr

Department of Electronics and Radio Engineering, Institute for Wearable Convergence Electronics, Kyung Hee University, 1 Seocheon-dong, Giheung-gu, Yongin-si, Gyeonggi-do 446-701, Republic of Korea

crystal structure ( $\beta$ - $\text{Ga}_2\text{O}_3$ ) after calcination [22, 23]. The crystal structures of  $\text{Ga}_2\text{O}_3$  nanostructures strongly affect the chemical property and photocatalytic activity, but they still have not been completely studied. In this work, we prepared and characterized two kinds of  $\text{Ga}_2\text{O}_3$  nanorods ( $\alpha$ - and  $\beta$ -crystal structures) via a facile hydrothermal synthesis and proper calcination. By changing the temperature of the growth solution, the morphological properties of GaOOH nanostructures were investigated. Previously, there are so many reports on the preparation of  $\text{Ga}_2\text{O}_3$  nanorods by hydrothermal and solvothermal methods which include complex instruments, making it an expensive approach. Girija et al. synthesized  $\text{Ga}_2\text{O}_3$  nanostructures by the reflux method [24], Li et al. and Wang et al. used hydrothermal synthesis (autoclave) [25, 26], and Zhang et al. used the solvothermal method (autoclave) to obtain the  $\text{Ga}_2\text{O}_3$  nanostructures [27]. However, in this work, we chose a simple and cost-effective process in which a beaker on a hotplate is used to produce crystalline  $\text{Ga}_2\text{O}_3$  nanostructures. To characterize the structural property and functional group of the prepared samples, field-emission scanning electron microscopy (FE-SEM), X-ray diffraction (XRD), transmission electron microscopy (TEM), and Fourier transform infrared spectroscopy (FT-IR) analyses were employed. Also, the photocatalytic feasibility of  $\text{Ga}_2\text{O}_3$  nanorods was evaluated by measuring the UV-vis absorption spectrum with a Rhodamine B (RhB) solution for environmental applications.

## Methods

The GaOOH nanorods were synthesized by the hydrothermal synthesis method using analytical pure grade chemicals. To make the growth solution, 0.1 M of gallium(III) nitrate hydrate ( $\text{Ga}(\text{NO}_3)_3 \cdot n\text{H}_2\text{O}$ ) was dissolved in 100 ml of de-ionized (DI) water. Then, the aqueous solution was heated on a hot plate at different temperatures from room temperature to 95 °C. While the temperature of the growth solution was maintained, ammonium hydroxide ( $\text{NH}_4\text{OH}$ ) was slowly added into the solution until a pH of 9 is reached. The final solution was then heated for 5 h to get a white precipitate of GaOOH nanorods. After the solution was naturally cooled down to room temperature, the precipitate was filtered and washed with DI water. Then, the sample was dried in an oven at 70 °C for 5 h under ambient atmosphere. Further, the as-prepared GaOOH nanorods were calcinated at different temperatures of 500, 800, and 1000 °C for 3 h to obtain the  $\alpha$ - and  $\beta$ - $\text{Ga}_2\text{O}_3$  powders.

For the morphological and structural analysis, FE-SEM (LEO SUPRA 55, Carl Zeiss), TEM (JEM-2100F, JEOL), and XRD (M18XHF-SRA, Mac Science) measurements were utilized. The thermal behavior of the GaOOH nanorods was investigated by thermogravimetric analysis-differential scanning calorimetry (TGA-DSC: SDT Q600 V8.3 Build 101). The FT-IR spectrum was scanned and analyzed in the wavenumber range of 4000–400  $\text{cm}^{-1}$  by using a FT-IR measurement system (Spectrum 100, PerkinElmer).

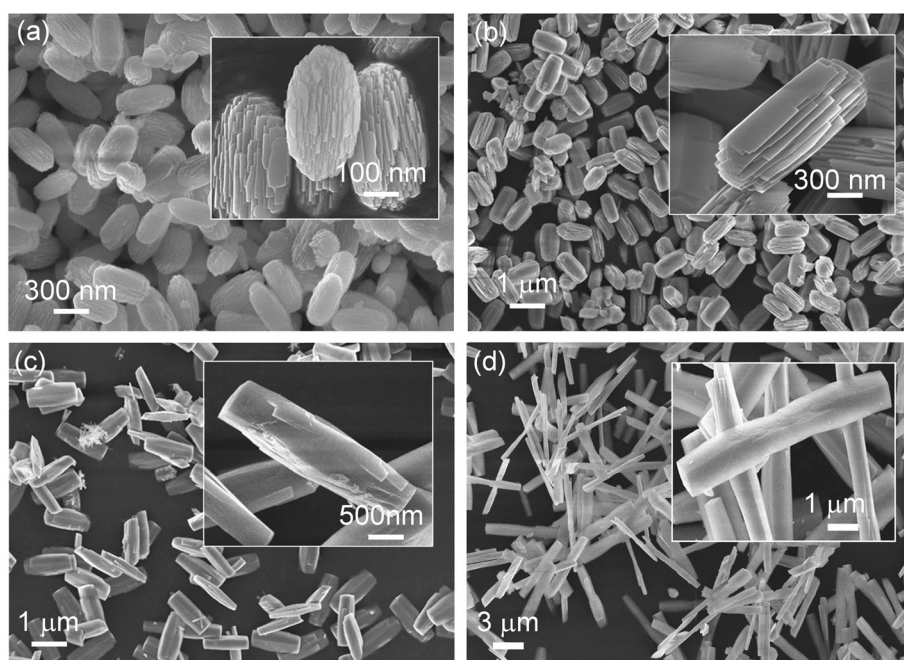


**Fig. 1** Effect of reaction temperature on the morphology of GaOOH nanostructures. FE-SEM images of the grown GaOOH nanostructures via hydrothermal method with different growth temperatures of **a** room temperature, **b** 50 °C, **c** 75 °C, and **d** 95 °C for 5 h

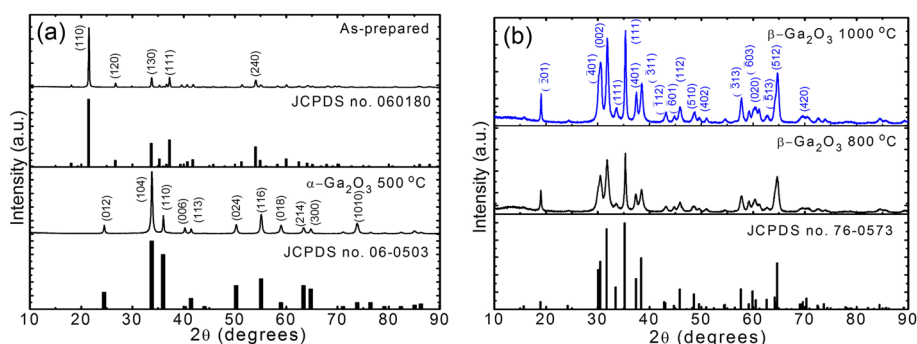


**Fig. 2** XRD of samples calcinated at different temperatures.  $2\theta$  scanned XRD patterns of **a** the as-prepared GaOOH nanorods and  $\alpha$ -Ga<sub>2</sub>O<sub>3</sub> calcined at 500 °C for 3 h and **b** the  $\beta$ -Ga<sub>2</sub>O<sub>3</sub> calcined at 800 and 1000 °C for 3 h. Here, the GaOOH nanorods were hydrothermally grown at 95 °C

The photocatalytic properties of  $\alpha$ - and  $\beta$ -Ga<sub>2</sub>O<sub>3</sub> nanorods for the degradation of Rhodamine B (RhB) aqueous solution were characterized by measuring the absorbance of the irradiated solution. For UV irradiation, the 100-W UV lamp (SXT-20-M, UVitec) was used as a light source. To prepare the suspension of the photocatalyst, 50 mg of Ga<sub>2</sub>O<sub>3</sub> nanorod powders was mixed with 50 ml of RhB aqueous solution ( $2 \times 10^{-4}$  M), which was continuously stirred at room temperature in the dark for 30 min. Then, the suspension was irradiated at different illumination times from 30 to 180 min. After that, the aliquot was separated from Ga<sub>2</sub>O<sub>3</sub> nanorod powders by using a filter paper and then the absorbance of RhB solution was obtained using a UV-vis spectrophotometer (CARY 300 Bio, Varian).

## Results and Discussion

Figure 1 shows the FE-SEM images of GaOOH nanostructures synthesized via the hydrothermal method with different growth temperatures of (a) room temperature, (b) 50 °C, (c) 75 °C, and (d) 95 °C for 5 h. In general, the growth temperature plays an important role in controlling the size and shape of GaOOH nanostructures during the hydrothermal process. As shown in Fig. 1a, the cocoon-shaped GaOOH nanostructures were formed at room temperature and their size was approximately 100 nm. These cocoon-shaped structures were formed by multi-layers of small nanoplates. As the growth temperature was increased to 50 °C, the nanoplates merge together with the increase in thickness and width of each nanoplate due to Ostwald's ripening as seen in Fig. 1b. Ostwald's ripening continues further when the growth temperature is up to 75 °C and the multi-layered stacked structures were converted to a rod-shaped structure (Fig. 1c). With further increase of the growth solution temperature (95 °C), nanorods grow lengthwise and the width of the rods decreases as can be seen in Fig. 1d. The inset of Fig. 1d shows a single nanorod with lengths of a few micrometers and widths of approximately 1  $\mu$ m. From the inset, we can also observe that the nanorod is

ready to split into two rods of smaller size if the temperature of the growth solution is further increased.

Figure 2 shows the  $2\theta$  scanned XRD patterns of (a) the as-prepared GaOOH nanorods and  $\alpha$ -Ga<sub>2</sub>O<sub>3</sub> calcined at 500 °C and (b) the  $\beta$ -Ga<sub>2</sub>O<sub>3</sub> calcined at 800 and 1000 °C for 3 h. Here, the GaOOH nanorods were hydrothermally grown at 95 °C. As shown in Fig. 2a, the measured

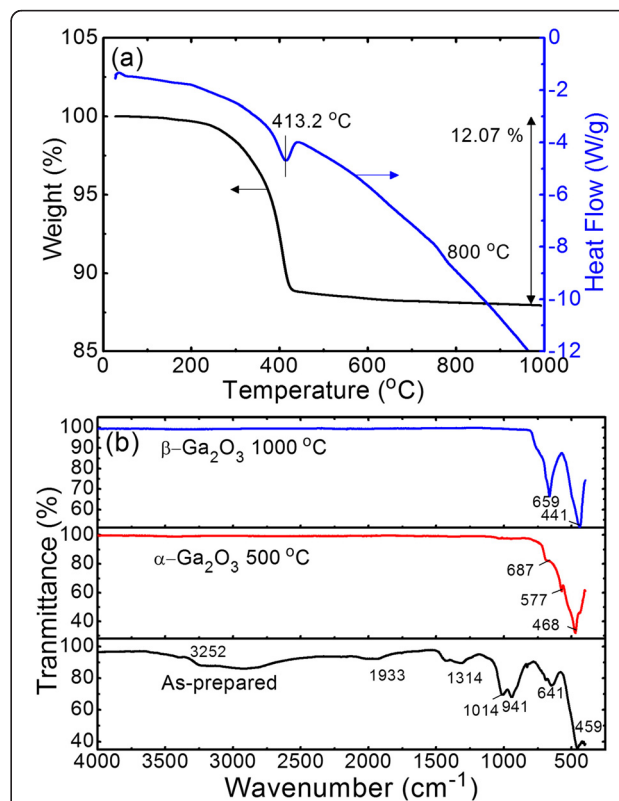


**Fig. 3** TGA-DSC curve and FT-IR spectra. **a** Measured TGA-DSC curves of the as-prepared GaOOH nanorods by heating from room temperature to 1000 °C with a fixed rate of 10 °C/min in a nitrogen atmosphere and **b** measured FT-IR spectra in the range of 4000 to 400  $\text{cm}^{-1}$  for the as-prepared GaOOH,  $\alpha$ -Ga<sub>2</sub>O<sub>3</sub>, and  $\beta$ -Ga<sub>2</sub>O<sub>3</sub> nanorods



XRD peaks of the as-prepared GaOOH material well agreed with the crystallized orthorhombic structure (JCPDS no. 06-0180). The sharp dominant peak of the crystal planes (110), (130), (111), and (240) were observed at  $2\theta = 21.5, 33.7, 37.2,$  and  $54.02^\circ$ , respectively. For the calcined sample at  $500^\circ\text{C}$ , it was observed that the as-prepared GaOOH nanorods were converted into  $\alpha\text{-Ga}_2\text{O}_3$  of the orthorhombic structure (JCPDS no. 06-0503) with dominant XRD peaks of (104) and (110) planes. When the calcination temperature was increased above  $500^\circ\text{C}$ , as shown in Fig. 2b, the samples were changed into a monoclinic  $\beta\text{-Ga}_2\text{O}_3$  (JCPDS no. 76-0573) without any impurity peaks. As the calcination temperature was increased to  $1000^\circ\text{C}$ , the XRD patterns were clearly enhanced with sharp peaks owing to the improved crystallinity at relatively high calcination temperature. The sharp dominant peaks of the ( $\bar{4}01$ ), (002), (111), and (512) planes were observed at  $2\theta = 30.4, 31.8, 35.3,$  and  $64.71^\circ$ , respectively.

Figure 3a shows the measured TGA-DSC curves of the as-prepared GaOOH nanorods by heating from room temperature to  $1000^\circ\text{C}$  with a fixed rate of  $10^\circ\text{C}/\text{min}$  in a nitrogen atmosphere. In the TGA curve of GaOOH, the total weight loss was 12.07 % from  $200$  to  $800^\circ\text{C}$  from the weight loss step process due to the physical removal of the absorbed water on the surface of GaOOH. For the endothermic peaks at  $413.2^\circ\text{C}$  in the

DSC curve, the phase transformation of GaOOH into  $\alpha\text{-Ga}_2\text{O}_3$  is well consistent with the measured XRD patterns of Fig. 2a. The weak endothermic peak was also observed at the temperature between  $750$  and  $830^\circ\text{C}$  with a weight loss of 2 % for the conversion from  $\alpha\text{-Ga}_2\text{O}_3$  to  $\beta\text{-Ga}_2\text{O}_3$  phase in the DSC curve. With further prolonged heating up to  $1000^\circ\text{C}$ , there is no weight loss. Figure 3b shows the measured FT-IR spectra in the range of  $4000$  to  $400\text{ cm}^{-1}$  for the as-prepared GaOOH,  $\alpha\text{-Ga}_2\text{O}_3$ , and  $\beta\text{-Ga}_2\text{O}_3$  nanorods. The as-prepared GaOOH exhibited two broad band peaks around  $3252.17$  and  $1932.62\text{ cm}^{-1}$  which are assigned to the stretching vibration of H-O-H bands. Also, the stretching vibration bond of the O-H group is also observed around  $1314\text{ cm}^{-1}$  owing to the absorption of water molecules. The constitutional bending vibration of Ga-OH bands was observed at  $1014$  and  $941\text{ cm}^{-1}$ . As the sample was calcined above  $500^\circ\text{C}$ , the peaks disappeared in the range of  $4000\text{--}700\text{ cm}^{-1}$  due to the dehydration of water molecules. For the  $\alpha\text{-Ga}_2\text{O}_3$  nanorods calcined at  $500^\circ\text{C}$ , the weak stretching peaks of the Ga-O band were observed at  $687, 577,$  and  $468\text{ cm}^{-1}$ , respectively. In contrast, the  $\beta\text{-Ga}_2\text{O}_3$  nanorods calcined at  $1000^\circ\text{C}$  clearly revealed the strong and narrow peaks at  $659$  and  $441\text{ cm}^{-1}$ , respectively. These FT-IR results well agreed with the trend of crystallinity for the  $\text{Ga}_2\text{O}_3$

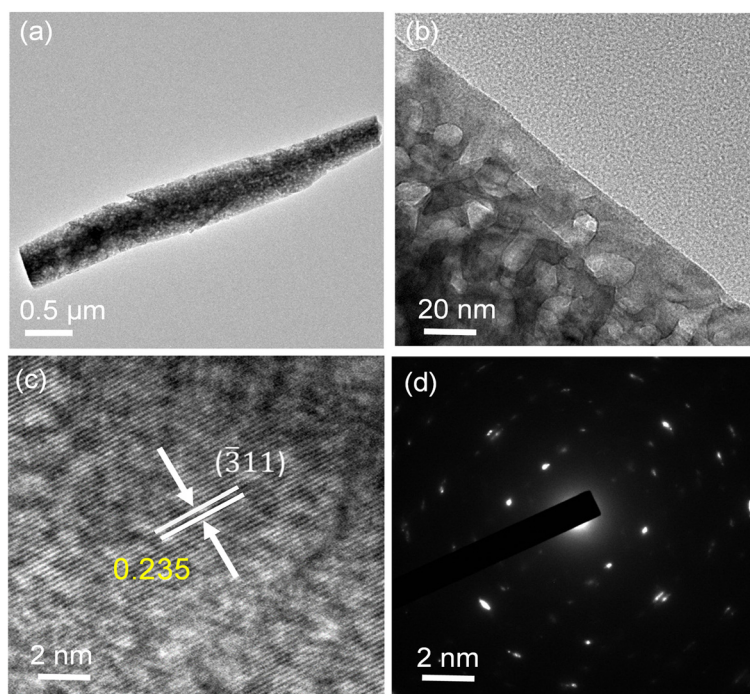


**Fig. 4** TEM images of  $\beta\text{-Ga}_2\text{O}_3$  nanorods. **a, b** TEM images and **c** HRTEM image of the calcined  $\beta\text{-Ga}_2\text{O}_3$  nanorods at  $1000^\circ\text{C}$ . The SAED pattern of the corresponding sample is shown in **d**

nanorods with different calcination temperatures from the XRD data (Fig. 2).

Figure 4 shows the TEM images and selected area electron diffraction (SAED) patterns of  $\beta$ - $\text{Ga}_2\text{O}_3$  nanorods calcined at 1000 °C. As can be seen in the perspective view of the TEM image (Fig. 4a), the single  $\beta$ - $\text{Ga}_2\text{O}_3$  nanorod exhibited a length of  $\sim 3 \mu\text{m}$  and a diameter of  $\sim 280$ – $400 \text{ nm}$  with many nanoholes. The porous structure of  $\beta$ - $\text{Ga}_2\text{O}_3$  nanorods was also previously reported by Liu et al. and Prakasham et al. [28, 29]. This pore surface of  $\beta$ - $\text{Ga}_2\text{O}_3$  nanorods was formed during the decomposition since water molecules were eliminated, thus leading to the creation of a lot of vacancies. In Fig. 4b, the many holes had a size of  $\sim 20 \text{ nm}$ , as clearly observed in the high-magnification view of the TEM image. From

the high-resolution TEM (HRTEM) images in Fig. 4c, the line array of lattice fringes ( $\bar{3}11$ ) was measured with a spacing of  $d = 0.235 \text{ nm}$ , which is reasonable in comparison with the measured crystal plane of the corresponding XRD peak. From the SAED pattern of  $\beta$ - $\text{Ga}_2\text{O}_3$  nanorods, it was also supported that the  $\text{GaOOH}$  nanorods could be well converted into the  $\beta$ - $\text{Ga}_2\text{O}_3$  phase with good crystallinity by calcinating at 1000 °C.

To examine the photocatalytic activity of  $\alpha$ - $\text{Ga}_2\text{O}_3$  and  $\beta$ - $\text{Ga}_2\text{O}_3$  nanorods, the photodegradation of RhB solution containing each sample was characterized. Figure 5 shows the measured absorbance spectra of the RhB solution at different UV irradiation times in the presence of (a) (i)  $\alpha$ - $\text{Ga}_2\text{O}_3$  and (ii)  $\beta$ - $\text{Ga}_2\text{O}_3$  nanorods. From both the absorbance spectra, it is commonly observed that

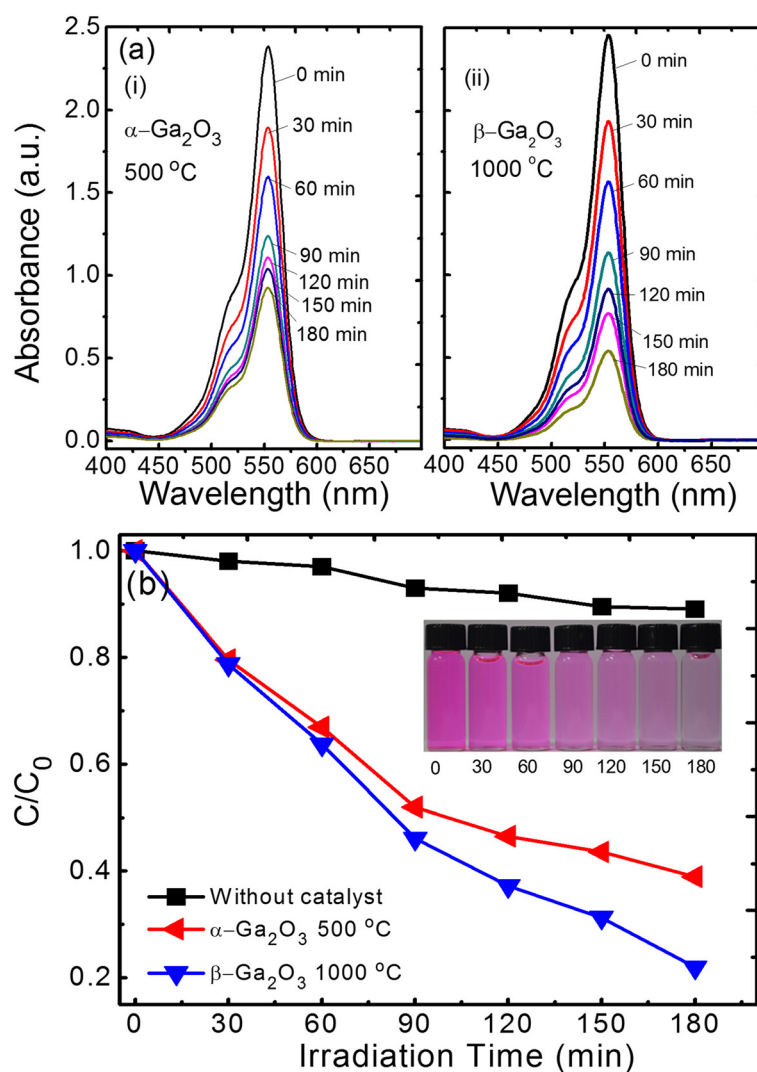


**Fig. 5** Photocatalytic activity of  $\alpha$ - $\text{Ga}_2\text{O}_3$  and  $\beta$ - $\text{Ga}_2\text{O}_3$  under UV irradiation. Measured absorbance spectra of the RhB solution at different UV irradiation times in the presence of **a** (i)  $\alpha$ - $\text{Ga}_2\text{O}_3$  and (ii)  $\beta$ - $\text{Ga}_2\text{O}_3$  nanorods. **b** Calculated constant reaction rate of the photodegradation of RhB solution ( $C/C_0$ ) as a function of UV irradiation time for  $\alpha$ - $\text{Ga}_2\text{O}_3$  and  $\beta$ - $\text{Ga}_2\text{O}_3$  nanorods. The photographic images of the RhB solution with  $\beta$ - $\text{Ga}_2\text{O}_3$  nanorods at different UV irradiation times are also shown in the inset of **b**

the absorption maximum of RhB occurred at 553 nm. As the UV irradiation time was increased from 0 to 60 min, the  $\alpha$ -Ga<sub>2</sub>O<sub>3</sub> and  $\beta$ -Ga<sub>2</sub>O<sub>3</sub> nanorods exhibited a similar degradation of the absorption maximum. However, the absorbance peak of  $\alpha$ -Ga<sub>2</sub>O<sub>3</sub> nanorods was slowly reduced for longer UV irradiation time than 90 min. Meanwhile, the RhB solution shows the steady photodegradation up to 180 min of UV irradiation time by the photocatalyst of  $\beta$ -Ga<sub>2</sub>O<sub>3</sub> nanorods. In general, the photocatalytic adsorption and desorption equilibrium are followed by a well-known Langmuir-Hinshelwood mechanism [30]. When the photon was absorbed into the photocatalyst, the photogenerated electron-hole separation contributed to the degradation of the RhB dye. Herein, this photocatalytic activity closely depends on the crystallinity and surface area [31–33]. The good crystallinity and porous surface of  $\beta$ -Ga<sub>2</sub>O<sub>3</sub> nanorods, from the XRD and TEM analyses (Figs. 2 and 4), led to the stable photocatalytic property compared to the  $\alpha$ -Ga<sub>2</sub>O<sub>3</sub> nanorods. Figure 5b shows the calculated constant reaction rate of the photodegradation of RhB solution ( $C/C_0$ ) as a function of UV irradiation time for  $\alpha$ -Ga<sub>2</sub>O<sub>3</sub> and  $\beta$ -Ga<sub>2</sub>O<sub>3</sub> nanorods. Here,  $C_0$  is the initial concentration of the RhB dye and  $C$  is the concentration of the UV-irradiated RhB solution. For comparison, the self-degradation rate of RhB solution was also shown by obtaining the  $C/C_0$  without photocatalyst. When the UV irradiation time was increased, the  $\beta$ -Ga<sub>2</sub>O<sub>3</sub> nanorods provided a more efficient constant reaction rate. At 180 min of UV irradiation time, the photodegradation efficiency reached to 62 and 79 % for the  $\alpha$ -Ga<sub>2</sub>O<sub>3</sub> and  $\beta$ -Ga<sub>2</sub>O<sub>3</sub> nanorods, respectively. The inset of Fig. 5b shows the photographic images of the RhB solution with  $\beta$ -Ga<sub>2</sub>O<sub>3</sub> nanorods at different UV irradiation times. As the UV irradiation time was increased, it is clearly observed that the initial pink color of the RhB solution gradually disappeared, exhibiting a colorless solution. These fabrication methods and characterizations suggest that hydrothermally synthesized  $\beta$ -Ga<sub>2</sub>O<sub>3</sub> nanorods can be expected to be a promising alternative for photocatalysts in the environmental remediation process.

## Conclusions

The GaOOH nanorods with a length of  $\sim 1$   $\mu$ m and a width of  $\sim 300$ – $400$  nm were successfully prepared by a simple hydrothermal synthesis at 95 °C of growth temperature. Then, the as-prepared GaOOH nanorods were calcined at different temperatures of 500–1000 °C for converting into single crystalline  $\alpha$ -Ga<sub>2</sub>O<sub>3</sub> and  $\beta$ -Ga<sub>2</sub>O<sub>3</sub> nanorods, and their crystal structures were confirmed by the XRD analysis. Also, the dehydration processes were studied by thermal analysis with consideration of the phase changes of the as-prepared GaOOH precursors. At 1000 °C of calcination temperature, the  $\beta$ -Ga<sub>2</sub>O<sub>3</sub> nanorods with good crystallinity and porous surface were

formed by the removal of water molecules during the dehydration. Additionally, these  $\beta$ -Ga<sub>2</sub>O<sub>3</sub> nanorods provided a relatively stable and high photocatalytic activity, compared with the  $\alpha$ -Ga<sub>2</sub>O<sub>3</sub> nanorods. Under UV irradiation for 180 min, the  $\beta$ -Ga<sub>2</sub>O<sub>3</sub> nanorods exhibited a relatively high photodegradation efficiency of 79 % compared to the  $\alpha$ -Ga<sub>2</sub>O<sub>3</sub> nanorods (62 %). This fabrication process and analysis can be useful to produce a good inorganic semiconductor nanomaterial-based photocatalyst.

## Competing Interests

The authors declare that they have no competing interests.

## Authors' Contributions

LSR designed and analyzed the Ga<sub>2</sub>O<sub>3</sub> nanorod photocatalysis (in RhB solution) experiment. YHK assisted in the synthesis and measurements (UV-vis, TEM). JSY supervised the conceptual framework and drafted the manuscript. All authors read and approved the final manuscript.

## Acknowledgements

This work was supported by the National Research Foundation of Korea (NRF) grant funded by the Korea government (MSIP) (No. 2015-023255).

Received: 9 June 2015 Accepted: 6 September 2015

Published online: 16 September 2015

## References

1. Benjwal P, Kar KK. Simultaneous photocatalysis and adsorption based removal of inorganic and organic impurities from water by titania/activated carbon/carbonized epoxy nanocomposite. *J Environ Chem Eng.* 2015;3(3):2076–83.
2. Dong H, Zeng G, Tang L, Fan C, Zhang C, He X, et al. An overview on limitations of TiO<sub>2</sub>-based particles for photocatalytic degradation of organic pollutants and the corresponding countermeasures. *Water Res.* 2015;79:128–46.
3. Rajeshwar K, Thomas A, Janáky C. Photocatalytic activity of inorganic semiconductor surfaces: myths, hype, and reality. *J Phys Chem Lett.* 2015;6(1):139–47.
4. Ramanathan R, Bansal V. Ionic liquid mediated synthesis of nitrogen, carbon and fluorine-codoped rutile TiO<sub>2</sub> nanorods for improved UV and visible light photocatalysis. *RSC Adv.* 2015;5(2):1424–9.
5. Yu H, Jin B, Feng C, Bi Y, Jiao Z, Lu G. Facile synthesis of Ag<sub>3</sub>PO<sub>4</sub> nanospheres with enhanced photocatalytic properties for the degradation of methylene blue under visible light irradiation. *Nanosci Nanotechnol Lett.* 2015;7(7):565–70.
6. Cao Y, Xu Y, Hao H, Zhang G. Room temperature additive-free synthesis of uniform Cu<sub>2</sub>O nanocubes with tunable size from 20 nm to 500 nm and photocatalytic property. *Mater Lett.* 2014;114:88–91.
7. Cao F, Lv X, Ren J, Miao L, Wang J, Li S et al. Preparation of uniform BiOI nanoflowers with visible light-induced photocatalytic activity. *Aust J Chem.* 2015. <http://dx.doi.org/10.1071/CH15176>.
8. Kang BK, Lim HD, Mang SR, Song KM, Jung MK, Kim S-W, et al. Synthesis and characterization of monodispersed  $\beta$ -Ga<sub>2</sub>O<sub>3</sub> nanospheres via morphology controlled Ga<sub>4</sub>(OH)<sub>10</sub>SO<sub>4</sub> precursors. *Langmuir.* 2015;31(2):833–8.
9. Tachikawa T, Majima T. Metal oxide mesocrystals with tailored structures and properties for energy conversion and storage applications. *NPG Asia Mater.* 2014;6:e100.
10. Veres A, Menesi J, Janaky C, Samu GF, Scheyer MK, Xu Q, et al. New insights into the relationship between structure and photocatalytic properties of TiO<sub>2</sub> catalysts. *RSC Adv.* 2015;5(4):2421–8.
11. Liu T-J, Wang Q, Jiang P. Morphology-dependent photo-catalysis of bare zinc oxide nanocrystals. *RSC Adv.* 2013;3(31):12662–70.
12. Han X-G, He H-Z, Kuang Q, Zhou X, Zhang X-H, Xu T, et al. Controlling morphologies and tuning the related properties of nano/microstructured ZnO crystallites. *J Phys Chem C.* 2009;113(2):584–9.
13. Muruganandham M, Amutha R, Wahed MSMA, Ahmmad B, Kuroda Y, Suri RPS, et al. Controlled fabrication of  $\alpha$ -GaOOH and  $\alpha$ -Ga<sub>2</sub>O<sub>3</sub> self-assembly and its superior photocatalytic activity. *J Phys Chem C.* 2012;116(1):44–53.

14. Jin C, Park S, Kim H, Lee C. Ultrasensitive multiple networked Ga<sub>2</sub>O<sub>3</sub>-core/ZnO-shell nanorod gas sensors. *Sens Actuators, B*. 2012;161(1):223–8.
15. Sheng T, Liu X-Z, Qian L-X, Xu B, Zhang Y-Y. Photoelectric properties of β-Ga<sub>2</sub>O<sub>3</sub> thin films annealed at different conditions. *Rare Met*. 2015;1–5
16. Zhao W, Xi H, Zhang M, Li Y, Chen J, Zhang J, et al. Enhanced quantum yield of nitrogen fixation for hydrogen storage with in situ-formed carbonaceous radicals. *Chem Commun*. 2015;51(23):4785–8.
17. Xu X, Bi K, Huang K, Liang C, Lin S, Wang WJ, et al. Controlled fabrication of α-GaOOH with a novel needle-like submicron tubular structure and its enhanced photocatalytic performance. *J Alloys Compd*. 2015;644:485–90.
18. Meng S, Danzhen L, Wenjuan Z, Xianzhi F, Yu S, Wenjuan L, et al. Rapid microwave hydrothermal synthesis of GaOOH nanorods with photocatalytic activity toward aromatic compounds. *Nanotechnology*. 2010;21(35):355601.
19. Li G, Peng C, Li C, Yang P, Hou Z, Fan Y, et al. Shape-controllable synthesis and morphology-dependent luminescence properties of GaOOH:Dy<sup>3+</sup> and β-Ga<sub>2</sub>O<sub>3</sub>:Dy<sup>3+</sup>. *Inorg Chem*. 2010;49(4):1449–57.
20. Zhao Y, Frost RL, Yang J, Martens WN. Size and morphology control of gallium oxide hydroxide GaO(OH), nano- to micro-sized particles by soft-chemistry route without surfactant. *J Phys Chem C*. 2008;112(10):3568–79.
21. Qian H-S, Gunawan P, Zhang Y-X, Lin G-F, Zheng J-W, Xu R. Template-free synthesis of highly uniform α-GaOOH spindles and conversion to α-Ga<sub>2</sub>O<sub>3</sub> and β-Ga<sub>2</sub>O<sub>3</sub>. *Cryst Growth Des*. 2008;8(4):1282–7.
22. Chai X, Liu Z, Huang Y. Influence of PEG 6000 on gallium oxide (Ga<sub>2</sub>O<sub>3</sub>) polymorphs and photocatalytic properties. *Sci China Chem*. 2015;58(3):532–8.
23. Pandey RM, Naidu BS, Sudarsan V, Pandey M, Kshirsagar RJ, Vatsa RK. Synthesis and characterization of Ga<sub>2</sub>O<sub>3</sub>:Eu nanorods. *AIP Conference Proceedings*. 2015;1665(1):140053.
24. Girija K, Thirumalairajan S, Mangalaraj D. Morphology controllable synthesis of parallelly arranged single-crystalline β-Ga<sub>2</sub>O<sub>3</sub> nanorods for photocatalytic and antimicrobial activities. *Chem Eng J*. 2014;236:181–90.
25. Li D, Duan X, Qin Q, Fan H, Zheng W. Ionic liquid-assisted synthesis of mesoporous α-Ga<sub>2</sub>O<sub>3</sub> hierarchical structures with enhanced photocatalytic activity. *Journal of Materials Chemistry A*. 2013;1(40):12417–21.
26. Wang Y, Li N, Duan P, Sun X, Chu B, He Q. Properties and photocatalytic activity of β-Ga<sub>2</sub>O<sub>3</sub> nanorods under simulated solar irradiation. *J Nanomater*. 2015;2015:5.
27. Zhang W, Naidu BS, Ou JZ, O'Mullane AP, Chrimes AF, Carey BJ, et al. Liquid metal/metal oxide frameworks with incorporated Ga<sub>2</sub>O<sub>3</sub> for photocatalysis. *ACS Appl Mater Interfaces*. 2015;7(3):1943–8.
28. Liu J, Zhang G. Mesoporous mixed-phase Ga<sub>2</sub>O<sub>3</sub>: green synthesis and enhanced photocatalytic activity. *Mater Res Bull*. 2015;68:254–9.
29. Arul Prakasam B, Lahtinen M, Muruganandham M, Sillanpää M. Synthesis of self-assembled α-GaOOH microrods and 3D hierarchical architectures with flower like morphology and their conversion to α-Ga<sub>2</sub>O<sub>3</sub>. *Mater Lett*. 2015;158:370–2.
30. Dong S, Zhang X, He F, Dong S, Zhou D, Wang B. Visible-light photocatalytic degradation of methyl orange over spherical activated carbon-supported and Er<sup>3+</sup>:YAlO<sub>3</sub>-doped TiO<sub>2</sub> in a fluidized bed. *J Chem Technol Biotechnol*. 2015;90(5):880–7.
31. Cheng H, Wang J, Zhao Y, Han X. Effect of phase composition, morphology, and specific surface area on the photocatalytic activity of TiO<sub>2</sub> nanomaterials. *RSC Adv*. 2014;4(87):47031–8.
32. Zhao Z, Wang Y, Xu J, Shang C, Wang Y. AgCl-loaded mesoporous anatase TiO<sub>2</sub> with large specific surface area for enhancing photocatalysis. *Appl Surf Sci*. 2015;351:416–24.
33. Liu H, Joo JB, Dahl M, Fu L, Zeng Z, Yin Y. Crystallinity control of TiO<sub>2</sub> hollow shells through resin-protected calcination for enhanced photocatalytic activity. *Energy Environ Sci*. 2015;8(1):286–96.

Submit your manuscript to a SpringerOpen® journal and benefit from:

- Convenient online submission
- Rigorous peer review
- Immediate publication on acceptance
- Open access: articles freely available online
- High visibility within the field
- Retaining the copyright to your article

---

Submit your next manuscript at ► [springeropen.com](http://springeropen.com)